IEEE Access
Multidisciplinary | Rapid Review | Open Access Journal

Received August 9, 2019, accepted August 23, 2019, date of publication August 29, 2019, date of current version September 13, 2019.

Digital Object Identifier 10.1109/ACCESS.2019.2938420

Influencing Factors of Flow Field of Ionic Wind Induced by Corona Discharge in a Multi-Needle-to-Net Electrode Structure Under Direct-Current Voltage

FANGCHENG LV, JINGXUAN SONG, PING WANG, HAOOU RUAN, AND JIANGHAI GENG
Hebei Provincial Key Laboratory of Power Transmission Equipment Security Defense, North China Electric Power University, Baoding 071003, China

Corresponding author: Ping Wang (pingwang0501@163.com)

This work was supported in part by the National Key Research and Development Program of China under Grant 2016YFB0900802, and in part by the Fundamental Research Funds for the Central Universities under Grant 2017MS101.

ABSTRACT The morphologies and velocity of ionic wind induced by direct-current (DC) corona discharge were experimentally measured. DC voltage was applied to short air gaps of high-voltage electrode–needle electrode and grounding electrode–net electrode to generate coronas, so as to allow the generation of ionic wind induced by corona discharge. The purpose of the study is to optimise the multi-needle-to-net electrode structure to improve the velocity of the ionic wind and keep it in a relatively stable state. For this purpose, the influences of various parameters on the velocity of the ionic wind were explored. The research results showed that the side length of meshes and the distribution mode of needles significantly affected the velocity of the ionic wind. The maximum velocity of the ionic wind, when the side length of meshes was 0.85 mm was 3 and 1.28 times those when the side lengths of the meshes were 2 and 0.425 mm, respectively. This indicated that there was an optimal side length that can maximise the velocity of the ionic wind. Increasing the number of needles and optimising the distribution mode of needles can effectively improve the velocity, that is, the improvement of the number and distribution uniformity of needles was conducive to increase the velocity of the ionic wind. Increasing the voltage amplitude can increase the velocity of the ionic wind, however, it was possible that noise was significant and in this case, the corresponding voltage cannot be considered as the working voltage of the ionic wind generator.

INDEX TERMS Corna diacharge, gap discharge, schlieren technique, multi-needle-to-net electrode.

I. INTRODUCTION

Ionic wind induced by corona discharge is generated according to the following process: in a stable high-voltage electric field, while applying a high voltage between two electrodes with greatly different curvatures, air near the electrode with the larger curvature is ionised to generate an electron avalanche if the applied voltage reaches the corona inception voltage; furthermore, the electrons and positive ions move to two opposite electrodes under the effect of the electric field force so as to drive the motion of air molecules, thus forming the ionic wind [1]–[4]. The generation of the ionic wind does not rely on mechanical rotating parts and offers the advantages of low power consumption and low noise emission, therefore, the ionic wind has become a novel method of chip cooling, which can improve heat-dissipation efficiency by 250% compared with traditional heat dissipation methods [5]. Ionic wind shows potential for application in chip cooling, pneumatic flow control, etc. The ionic wind fan, radiator, bar, and machine have been applied to various industries including electronics, plastic, silk-screen, prepress systems, and picture processing. The benefits of this research are thus apparent.

In 1709, Hauksbee first discovered the phenomenon of the ionic wind [6]. In 1899, through experiments, Chattock found the relationships of the ionic wind with voltage and current and therefore first explained the characteristics of the ionic wind theoretically [7]. In 1986, Sigmond proposed a theoretical model for the voltage and current of a needle-to-plate corona discharge system, which provides a theoretical basis for subsequent research on the ionic wind [8]. Zou *et al.* [9] and Bian *et al.* [10] summarised present measurement method for atmospheric ion mobilities in a DC corona discharge and analysed the impact of fluctuations of the measured ionized

The associate editor coordinating the review of this article and approving it for publication was Xue Zhou.

field and ion current density on the results of ion mobilities. Wang *et al.* [11] summarised various aspects including the characteristics of, and mechanism driving, the flow field of ionic wind. Moreau and Touchard [12] and Huang [13] found that the positive DC power supply was more suitable for the ionic wind system, and analyzed the voltage polarity and gap spacing, and discovered that in the same case, the velocity and efficiency of ionic wind generated by the needle-net structure were higher than that of the needle-ring structure. On this basis, the optimized arrangement of mesh size and electrode spacing could obtain the optimal solution of the experiment. Owesnek [14] analyzed that the airflow generated among each needle would affect each other, which resulted in an optimal electrode density for the distribution of the needle electrodes. Previous studies on the ionic wind by scholars have shown that the needle-net electrode can generate higher ionic wind velocity and heat dissipation efficiency. To improve the efficiency of the ionic wind, we set a number of parallel needle electrodes in a certain range to emit ionic wind. At the same time, considering that in order to reduce the obstruction to ionic wind, the low-voltage side electrode was replaced with the net electrode with good ventilation. So the authors used a multi-needle-to-net structure in this experiment to try to generate a higher velocity, and optimized the arrangement of the needles, and the side length of the net electrode. The influence of voltage amplitude on ionic wind velocity was explored under the positive HVDC power. A simulation model was built with COMOL Multiphysics to compare the movement of positive and negative ions and the shape of the ionic wind with the schlieren image obtained from the test. The experimental results are proved to be correct.

By using a Z-shaped reflective schlieren system and a high-speed camera system, the development track and velocity of the ionic wind generated in a multi-needle-to-net under direct-current (DC) voltage were observed. In the test, based on a multi-needle-to-net electrode, the influences of three variables on the velocity of the ionic wind and the morphologies of the flow field were investigated by changing the three variables (side length of meshes of net electrodes, distribution mode of needle electrodes, and voltage amplitude). The results were expected to provide a basis for optimisation and design of the ionic wind generator in industrial production.

II. GENERATION OF THE IONIC WIND

The motion of ionic wind mainly relies on the effect of electric field force and the electric field is determined by the Poisson's equation.

$$\nabla^2\varphi = -\nabla\cdot\boldsymbol{E} = -\frac{q}{\varepsilon} \tag{1}$$

where φ is the electric potential, q the electric charge density, and ε the electric permittivity ($= 8.8542 \times 10^{-12} F/m$ in the air). The intensity of the electric field $\boldsymbol{E}$ is given as:

$$\boldsymbol{E} = -\nabla\varphi \tag{2}$$

The charge is controlled by the following transport equation which represents current continuity.

$$\nabla\cdot\boldsymbol{J} + \frac{\partial q}{\partial t} = 0$$
$$\boldsymbol{J} = \mu_E \boldsymbol{E} q + \boldsymbol{v} q - D\nabla q \tag{3}$$

where μ_E is the ionic mobility ($=1.43\times10^{-4}$ m^2/V s for air), $\mathbf{v}$ the ionic wind velocity, and D the coefficient of ionic diffusion. The diffusion of charge is usually much lower than the drift and therefore negligible and the fluid convection effect can also be negligible if no strong enforced bulk flow appears in the field. Since the velocity of the ionic wind is low, incompressible gas flow is assumed. The conservation equations for the mass, momentum and energy are expressed as:

$$\nabla\cdot\boldsymbol{v} = 0 \tag{4}$$

$$\frac{\partial\rho\mathbf{v}}{\partial t} + \nabla\cdot(\rho\mathbf{v}\otimes\mathbf{v}) = -\nabla P + \nabla\cdot(\mu\nabla\mathbf{v}) + \boldsymbol{F} \tag{5}$$

$$\frac{\partial\rho C_P T}{\partial t} + \nabla\cdot(\rho\boldsymbol{v}C_P T) = \nabla\cdot(k\nabla T) + \sigma_E |E|^2 \tag{6}$$

where ρ is the fluid density, P the pressure, T the temperature, μ the viscosity, k the thermal conductivity, C_P the specific heat capacity, and σ_E the electrical conductivity.

In the ionic wind, there is no consideration of buoyancy and the density ρ is constant. The last term in the energy equation represents the Joule heating effect, which is usually insignificant. The body force appearing in the momentum equation represents the EHD force.

$$\boldsymbol{F} = q\boldsymbol{E} - \frac{|\boldsymbol{E}|^2\nabla\varepsilon}{2} + \frac{\nabla(\rho\frac{\partial\varepsilon}{\partial\rho}|\boldsymbol{E}|^2)}{2} \tag{7}$$

The first term on the right is the Coulomb force resulting from free charges in the ionic wind. The second term represents the dielectrophoretic force due to the non-uniform distribution of permittivity. The third term is the electrostrictive force due to the variation of permittivity caused by the ionic wind density variation. The last two terms can be ignored in single-phase flows-ionic wind. Thus, the Coulomb force is considered to be the main reason causing the movement of charges in the zone where the ionic wind appears, that is [16]:

$$\boldsymbol{F} = q\boldsymbol{E} \tag{8}$$

III. OBSERVATION PLATFORM OF THE IONIC WIND

The test platform for the ionic wind is mainly composed of three parts: an ionic wind generator; a high-speed camera system and a measuring system for the velocity of the ionic wind.

The ionic wind generator comprised three parts: a DC power supply, multi-needle-to-net electrodes, and an air gap. As for the DC power supply under a high voltage, the HT2332 programmable DC power supply produced by Beijing Henki was applied to generate and maintain the electric field. HT2332 was a high precision, high stability, low noise linear programmable DC power supply with independent three-channel output. 2 bit D/A converter to control

output voltage and current By using the interference principle of coherent light, schlieren images featured the change of flow field of the zone to be measured as light and dark stripes on the optical screen, thus capturing the transparent flow field which is otherwise difficult to observe [17]–[19]. The high-speed shooting system consists of a Z-shaped reflective schlieren and a Fastec Imaging IL5 high-speed camera, which had full HD frame rates 1000 fps. The height of the schlieren apparatus could be adjusted, and the maximum diameter of the observed flow field is 300 mm, which is limited by the dimension of the parabolic mirror. The structure of the Z-shaped reflective schlieren images used here was shown in Fig 1. During the test, the high-speed camera always synchronously photographed images and the images captured by the camera were sent to a computer through signal lines. Based on the Fastec FasMotion software in the computer, the image from the high-speed camera could be received. By applying related settings used for storage, 300 images before triggering, and 700 images after triggering, were stored, in which each image was named according to shooting time.

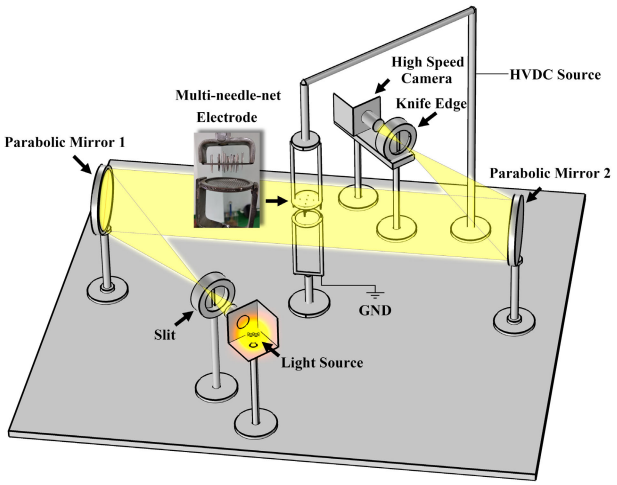

FIGURE 1. The structure of the Z-shaped reflective schlieren system.

The optical path and its mechanism were described as follows: the light emitted from the light source reached the parabolic mirror 1 through a slit. Afterwards, the parallel light was reflected to the parabolic mirror 2 through the parabolic mirror 1, in which the equivalent focus of the parabolic mirror 1 coincided with the slit and the parabolic mirror 2 coincided with the knife edge. A parallel light crossed, which completely covered the flow field to be measured, was formed between the parabolic mirror 1 and the parabolic mirror 2. Flow-field wave motions converged at the knife edge to form images at the high speed camera.

The ionic wind generator was of multi-needle-to-net form, in which needle electrodes were made of stainless steel, with a length of 50 mm, and the radius of curvature of needle tip was less than 0.10μm. Moreover, the diameter of the entire net electrode was 40 mm and the side length of meshes included 2, 0.85, and 0.425 mm, as shown in Fig 2(a). The ionic wind velocity was measured by placing a Smart Sensor

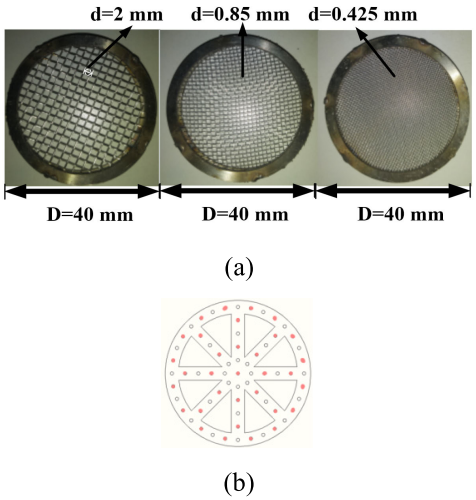

a) Net electrodes with the side lengths of meshes of 2, 0.85, and 0.425 mm;b) Distribution of needle electrodes

FIGURE 2. Distribution of net electrodes with different side lengths of meshes and needle electrodes.

split type anemometer 10 mm directly under the net electrode. Its measurement range was 0.3∼45 m/s, the resolution was 0.001 m/s, and the error was within 3%. Due to the strong electric field between the emitter and charge receiving electrode, the particles including the ions and neutral moleculars were almost all collected by the anemometer. The gap spacing was 30 mm and the ambient temperature was 25°C. The relative humidity was 40% and the velocity of background flow-field was less than 0.01m/s.

IV. FACTORS AFFECTING THE IONIC WIND IN A MULTI-NEEDLE-TO-NET ELECTRODE STRUCTURE

A. DESIGN OF A MULTI-NEEDLE-TO-NET ELECTRODE STRUCTURE

A needle electrode was vertically placed in each mesh. By changing the location, and number, of needle electrodes, the morphologies and velocity of the ionic wind were regulated. The middle hollow part of the disc can improve the aerodynamic performance of the ionic wind generator. The grounding net electrode structure appeared as a circular net whose diameter was slightly larger than that of the needle supporter supporting multi-needle electrode. In the test, the net electrodes with side lengths of meshes of 2, 0.85, and 0.425 mm were designed to explore the influence of the side length of meshes on performances of the ionic wind generator (Fig 2(a)).

The multi-needle-to-net electrodes were all made of stainless steel, and were separately bolted to the conductive supporter. The height of the supporter can thus be adjusted. The needle electrode was connected to the end of the DC power supply with a high voltage through power lines while the net electrode was grounded through grounding lines. When constantly applying a DC voltage, the ionic wind flowing along the axis of the multi-needle-to-net electrode structure was generated.

B. THE INFLUENCE OF THE SIDE LENGTH OF MESHES OF NET ELECTRODES ON THE IONIC WIND

To explore the influence of the side length of meshes of net electrodes on the working performances of the ionic wind generator, various parameters were set as follows: the gap spacing G was 30 mm; the diameter of entire net electrode D was 40 mm; the shape of net electrodes was shown as Fig 2(a); the distribution of needle electrodes was displayed in Fig 2(b) (The red dots indicated the position where the needle electrodes were placed). Owing to the velocity of the ionic wind under positive DC voltage being greater than nagetive DC voltage under the same voltage amplitude, the positive DC voltage was used as the power supply of the ionic wind generator [20]. The corona discharge process when constantly increasing the DC voltage amplitude in different side lengths of meshes is recorded in Table 1. The change of ionic wind velocity under different side lengths of meshes with voltage amplitude is shown in Fig 3. Under a voltage amplitude U_m = 44 kV, the schlieren photographs of the ionic wind under three side lengths of meshes were shown in Fig 4.

TABLE 1. The influence of the side length of meshes on breakdown voltage.

Side Length of Meshes *d* (mm)	2	0.85	0.425
Discharge Inception Voltage *Ud* (kV)	19.8	20.1	19.9
Voltage Range for High Corona Wind velocity *Ur* (kV)	40.5-44	39.9-45.5	41.5-44.5
Voltage at Which Corona Noise Begins to Appear *Us* (kV)	44	45.5	44.5
BreakdownVoltage*Ub* (kV)	55.3	55.5	55.8

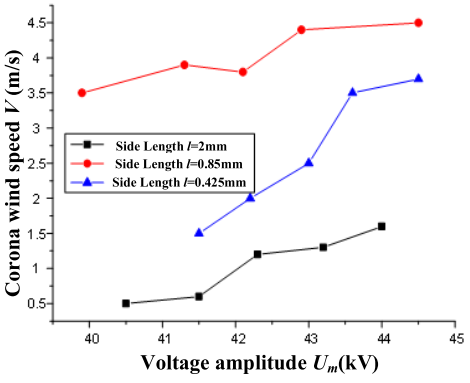

FIGURE 3. Ionic wind velocities under different side lengths of meshes.

As shown in Table 1, Figs 3, and 4, for three different side lengths of meshes of net electrodes, inception, increasing velocity of ionic wind, generating and growing noise induced by corona discharge as well as breakdown of the air gap successively occurred when increasing the applied voltage. Under the same voltage amplitude, the velocities of the ionic wind in the case of three side lengths of meshes are shown, in descending order, as $V_{i0.85}$, $V_{i0.425}$, and V_{i2}. It can be inferred that there was the optimal side length of meshes under certain conditions. Too large, or too small, a mesh side length inhibits the development of the ionic wind. On condition that the gap spacing was 30 mm, the entire diameter of net electrodes D was 40 mm and distribution 5 (shown in Fig.5e) was applied, the largest velocity of the ionic wind can be attained under the same voltage amplitude when using the net electrodes with the side length of meshes of 0.85 mm. Being restricted by experimental conditions, only three net electrodes with different side lengths of meshes were prepared. In subsequent tests, it was feasible to make multiple net electrodes with different side lengths of meshes for further research.

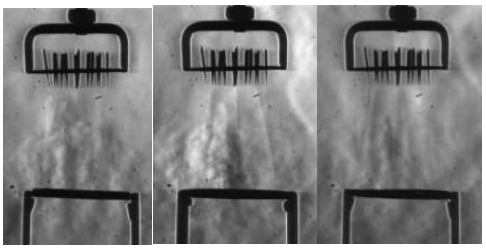

(a)side lengths=2mm(b)side lengths=0.85mm(c)side lengths=0.425mm

FIGURE 4. Ionic wind images for side lengths of meshes of 2, 0.85, and 0.425 mm.

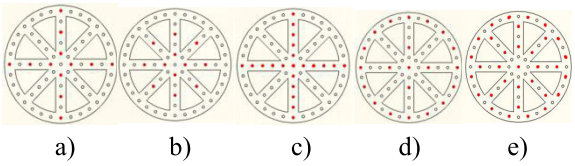

FIGURE 5. Five distributions of needle electrodes.

C. THE INFLUENCE OF THE NUMBER AND DISTRIBUTION OF NEEDLE ELECTRODES ONTHE IONIC WIND

To investigate the influence of the number and distribution mode of needle electrodes on performances of the ionic wind generator, the diameter of the entire net electrodes D = 40 mm, the side length of meshes d = 0.85 mm, and the gap spacing G = 70 mm. In addition, the numbers of needle electrodes were separately set to 12, 21, and 32, giving three types of schemes. Moreover, when the numbers of needle electrodes were set as 12 and 21, two distribution modes of needle electrodes were separately designed. As a result, there were five distributions: red dots denote the locations of needle electrodes in Fig.5.

Table 2 shows the statistical result of the velocities of the ionic wind under five distribution modes of needle electrodes obtained through multiple tests. By summarising the data in Table 2, the change in velocity of the ionic wind under different distributions of needle electrodes with voltage amplitude is attained (Fig 6). According to the figure, it can be seen that increasing the number of needle electrodes can

TABLE 2. Statistical result of the velocities of the ionic wind under five distribution modes of needle electrodes.

Distribution modes of needle electrodes	Distribution 1					Distribution 2					Distribution 3	
Voltage amplitude Um(kV)	41.3	42.6	42.9	43.1	44	41.3	42	42.7	43.3	43.9	40.1	40.8
velocities of the ionic wind Vi(m/s)	4.2	4.7	4.9	4.9	5.2	5.4	5.6	5.5	5.8	5.8	4.3	4.4
Distribution modes of needle electrodes	Distribution 3			Distribution 4				Distribution 5				
Voltage amplitude Um(kV)	41.4	41.9	42.8	40	41	41.3	42	42.5	40	40.8	42	42.5	43.5
velocities of the ionic wind Vi(m/s)	4.6	5	5.1	6.1	6.3	6.2	6.6	6.7	7.7	7.8	7.8	7.9	8

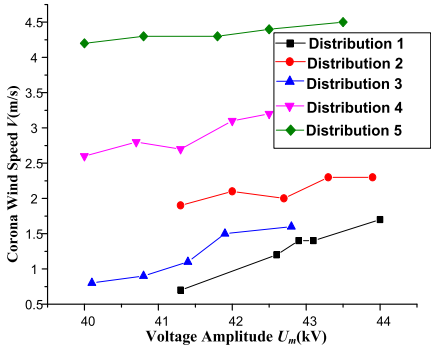

FIGURE 6. The ionic wind velocities for different distributions of needle electrodes.

accelerate the velocity of the ionic wind. It was supposed that the displacement current I in the air gap remained unchanged, charges were generated at the tip of the needle electrodes, and the charge density of the ionic wind generated due to multiple needle electrodes can be expressed as equation (9) [21].

$$\rho = nI/(\mu EA) \tag{9}$$

where, A, n, μ, and E denote the area of the tip of needle electrodes, the number of needle electrodes, charge mobility, and electric field intensity at the tip of needle electrodes, respectively. In air, the following result can be obtained according to Peek's law:

$$E = E_0(1 + 2.62 \times 10^{-2}/R^{1/2}) \tag{10}$$

where, R refers to the radius of curvature of the needle tip (unit: m). According to equation (10), it can be seen that the growth of the number of needle electrodes led to the increase of the number of charges between needle and net electrodes. The increasing inter-electrode charges were accumulated in the vicinity of needle electrodes. Moreover, under the effect of a downwards electric field, the positive ions moved to net electrodes, thus driving more neutral molecules towards the net electrode.

Additionally, given a predetermined number of needle electrodes, optimising the distribution thereof can also increase the velocity of the ionic wind. The more uniform the needle electrode distribution, the larger the ionic wind velocity. It can be also seen that under the distribution mode in distribution 5, the velocity of the ionic wind was the largest and then remained constant with increasing voltage amplitude. The result showed that the ionic wind generator with the uniform distribution of needle electrodes can inhibit the growth of external voltage to some extent and retain the stability of wind velocity, thus obtaining a wide zone with a uniform flow field where the ionic wind acted thereon. It can be seen that optimising the structure of needle electrodes can greatly increase the velocity of the ionic wind.

D. THE INFLUENCE OF VOLTAGE AMPLITUDE ON THE IONIC WIND IN MULTI-NEEDLE-TO-NET ELECTRODE COUPLES

To investigate the influence of voltage on performances of the ionic wind generator in a multi-needle-to-net electrode structure, a positive DC power supply was selected as the voltage source. Moreover, the gap spacing G was 80 mm and the side length of the meshes was 0.85 mm. Additionally, 32 needle electrodes were applied, which were distributed according to distribution 5. The schlieren photographs, taken as the voltage was increasing, were recorded. Fig 7 shows the images of the ionic wind when the voltages were 20, 40, 53, and 58 kV, respectively.

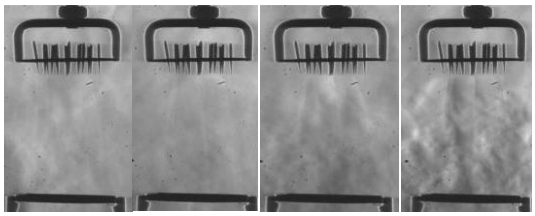

FIGURE 7. Schlieren photographs of ionic wind at different voltage amplitudes.

It can be seen from Fig 7 that, at a voltage amplitude of 20 kV, no significant airflow was generated between the electrodes. At a voltage amplitude of 40 kV, the channel for jet flow appeared; however, jet flow was insignificant and ionic wind caused little disturbance on the flow field. When the voltage amplitude increased beyond 40 kV, the increase in voltage influenced the change in the morphology of ionic wind. When the voltage amplitude was between 40 and 50 kV, the noise induced by coronal discharge gradually increased and it reached its peak at a voltage amplitude of 50 kV. When the voltage was between 50 to 53 kV, the noise gradually decreased and vanished when the voltage reached 53 kV. In this case, it can be seen that the air flow generated by the ionic wind changed the air flow field across the whole gap. When the voltage increased to 58 kV, noise induced by coronal discharge occurred again until the air gap breakdown at a voltage of 67 kV. When increasing the voltage amplitude, the change in the ionic wind velocity was as shown in Fig 8.

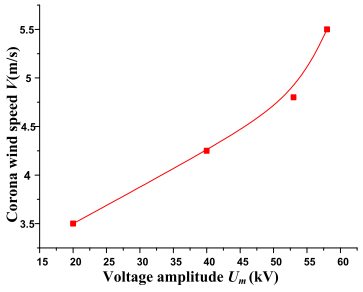

FIGURE 8. The change in ionic wind velocity when increasing the voltage amplitude.

The aforementioned phenomena revealed that the growth of voltage amplitude can directly influence the velocity of ionic wind. Within a certain voltage range, a high voltage amplitude was conducive to formation of ionic wind and therefore the velocity of the ionic wind increased with the voltage amplitude. The reason was that Coulomb force applied to the ions increased with the externally applied DC voltage so as to increase the velocity, thus greatly rising movement velocities of neutral molecules and positive ions: however, with the voltage increasing, the collisions of molecules and positive ions were aggravated with the increasing velocity. As a result, the noise induced by coronal discharge was likely to be loud. Therefore, it was inappropriate to apply the corresponding voltage amplitude in this context as the working voltage of the ionic wind generator. Hence, it was necessary to determine a voltage amplitude, under which there was low noise induced by coronal discharge and a high velocity of ionic wind, as the working voltage of the ionic wind generator.

E. MOVEMENT OF IONS UNDER POSITIVE DC VOLTAGE

In order to further analyze the morphology of ionic wind, the motion of charged particles in the gap is simulated by finite element method based on COMSOL Multiphysics. The coupling model consists of electrostatic field module and dilute transfer module. As an example, the needle electrodes composed of three needles and the net electrode whose side length= 0.85 mm were used. The positive DC voltage was applied in this experiment. For the electrostatic field module, three needles-net electrode was adopted to form the initial electric field. Three needle electrodes were applied with 55kV DC voltage, and the net electrode was grounded. Meanwhile, a circular area with diameter of 0.1 mm was set at the needle tip to simply simulate the corona discharge. The Poisson equation was used to calculate the electric field distribution in the gap.

For the dilute transfer module, the generation of charged particles is not only related to ionization and recombination in the air, but also to the generation of ion pairs in the corona region. The concentration of charged particles in space was calculated based on the drift diffusion equation as shown in equation (11):

$$\frac{\partial c_1}{\partial t} = \text{R-D}_1 \cdot \nabla^2 c_1 \text{-k}_c \text{N}_\text{A} c_1 c_2 - \nabla \cdot (b_1 c_1 \cdot \nabla \varphi) \quad (11)$$

where, c_1 and c_2 are the concentration of positive and negative charges in the gap respectively. The producing rate of particle concentration with time is determined by multiple factors. The first term (R) of the equation symbolizes the particle concentration generated by air ionization and corona discharge. The second, third and fourth terms respectively represent the density values reduced by gradient diffusion, positive and negative ion recombination, and electric field migration. Setting the needles and the net electrode as the inlet and outlet of charged particles, the time-varying concentration distribution of charged particles can be calculated.

In addition, the background electric field generated by charged particles is fed back to the electrostatic field module in real time through space charge coupling. Based on the finite model, We calculate the transient state of the above model with time as the main variable, and get the distribution change of charged particle density in the gap.

As can be seen from Figs. 9 and 10, in the ionic wind, the negative ions are mainly concentrated in a small area of corona near the needle electrodes. Because a positive voltage was applied to the needle electrodes, the negative ions were basically absorbed as soon as they are generated. Over time, positive ions were ejected from the needle electrodes, suggesting that the ionic wind was ejected from the more curvature electrode and moved toward the less curvature electrode. At T=1 ms, the corona radius was small and spherical.

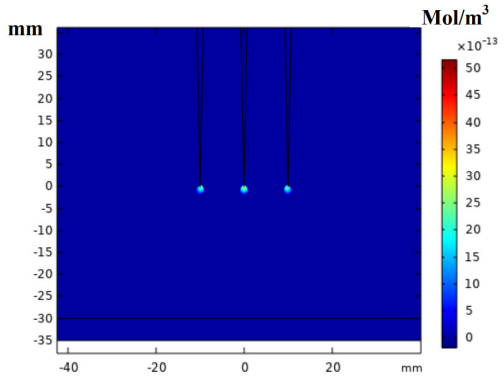

FIGURE 9. Distribution of negative ions when applying positive polarity voltage.

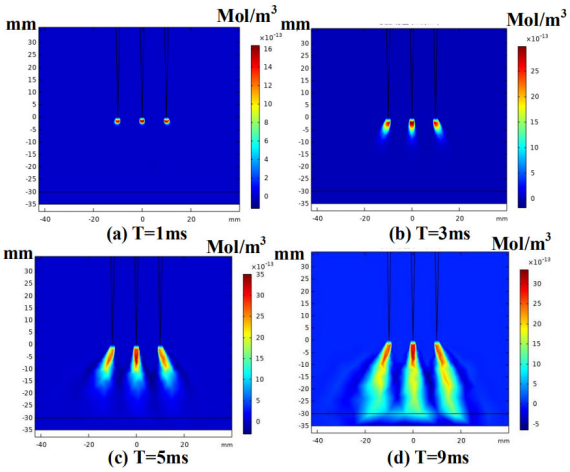

FIGURE 10. Distribution of positive ions at different time when applying positive polarity voltage.

With the further development of corona, under the electric field, the positive ions gradually moved downward, and the corona area became an ellipse instead of a sphere at T=3 ms, and finally moved to the net electrode at T=9 ms. In this process, there was always a trend: in the middle of the ionic wind channel, the positive ion density was the largest, and the positive ion density decreased outward successively. And the closer the ionic wind channel was to the needle electrode, the higher the positive ion density was, and there was no positive ion concentration near the net electrode. Moreover, the maximum concentration of positive ions occurs in the first third of the gap (near the needle electrodes), where the positive ion density was almost twice as much as that near the net electrode.

As can be seen from Fig.11, the width of the ionic wind channel keeps increasing with the direction away from the needle electrodes, and the distance between channels keeps decreasing, that is, the ionic wind channels composed of positive ions tend to merge with the direction away from the needle electrode. The concentration of charged particles obtained from the simulation results is similar to the morphological characteristics of the ionic wind obtained from the experiment.

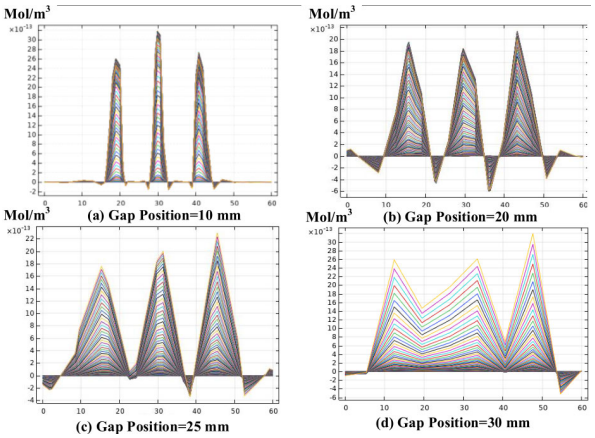

FIGURE 11. Distribution of positive ion concentration and channel width at different gap positions.

V. CONCLUSION

The nature of the motion and factors influencing ionic wind within a multi-needle-to-net electrode structure were investigated. We studied the motion of the positive and negative ions and the ionic wind movement trend under positive voltage. Moreover, the influences of the side length of meshes of net electrodes, distribution mode of needle electrodes, and voltage amplitude on the morphologies and velocity of the ionic wind were also analysed. Specific conclusions are drawn as follows:

1) Negative ions are mainly concentrated in the needle electrode (emitter), the positive ions moved towards the mesh electrode (charge receiving electrode) under the drive of the electric field. And the distribution of positive ions and the ionic wind form are very similar, so we could conclude that under the positive DC voltage, the ionic wind is formed by the positive ions driving the neutral molecules. And there is no charge buildup near the net electrode.
2) On condition of having the same side length of meshes of net electrodes, inception, increasing velocity of the ionic wind, noise generation, and noise growth induced by coronal discharge, and breakdown of the air gap, successively occurred when increasing the applied voltage. Under certain conditions, there was an optimal side length of meshes: too large, or too small, a mesh side length inhibited the development of the ionic wind.
3) Increasing the number of needle electrodes can increase the velocity of the ionic wind. Additionally, when having a determined number of needle electrodes, optimising the distribution of needle electrodes can also increase the velocity of the ionic wind. The more uniform the needle electrode distribution, the greater the velocity of the ionic wind.
4) Within a certain voltage range, a high voltage amplitude was conducive to the formation of the ionic wind, therefore, the velocity of the ionic wind increased with increasing voltage amplitude, except when the noise induced by coronal discharge was too loud.

5) It can be seen from the simulation results that the shape of the ionic wind can fit well with the Dilute transfer module and electrostatic field module, indicating that the ionic wind has less composition of plasma and is a weakly coupled movement of dispersed materials.

REFERENCES

[1] S. Park, U. Cvelbar, W. Choe, and S. Y. Moon, "The creation of electric wind due to the electrohydrodynamic force," *Nature Commun.*, vol. 9, no. 1, Jan. 2018, Art. no. 371.
[2] S. Golzari, A. Kasaeian, M. Amidpour, S. Nasirivatan, and S. Mousavi, "Experimental investigation of the effects of corona wind on the performance of an air-cooled PV/T," *Renew. Energy*, vol. 127, pp. 284–297, Nov. 2018.
[3] P. Wang, J. Song, H. Ruan, F. Lv, J. Geng, and X. Wang, "Development and morphological characterization of ion wind in an inhomogeneous DC field," *AIP Adv.*, vol. 9, no. 5, Apr. 2019, Art. no. 055002.
[4] S. Chen, F. Wang, Q. Sun, and R. Zeng, "Simulation of positive streamers in atmospheric air by a macroscopic model with a new branching criterion," *IEEE Trans. Dielectr. Elect. Insul.*, vol. 25, no. 6, pp. 2019–2110, Dec. 2018.
[5] S. Chen, R. G. W. van den Berg, and S Nijdam, "The effect of DC voltage polarity on ionic wind in ambient air for cooling purposes," *Plasma Sources Sci. Technol.*, vol. 27, no. 5, May 2018, Art. no. 055021.
[6] M. Robinson, "Movement of air in the electric wind of the corona discharge," *Trans. Amer. Inst. Elect. Eng., I, Commun. Electron.*, vol. 80, no. 2, pp. 143–150, May 2012.
[7] A. P. Chattock, "XLIV. On the velocity and mass of the ions in the electric wind in air," *London, Edinburgh, Dublin Philos. Mag. J. Sci.*, vol. 48, no. 294, pp. 401–420, 1899.
[8] R. S. Sigmond, "The unipolar corona space charge flow problem," *J. Electrostatics*, vol. 18, no. 3, pp. 249–272, Oct. 1986.
[9] Z. L. Zou, X. Cui, T. Lu, and X. Bian, "A measurement method for atmospheric ion mobilities based on cylindrical electrodes in direct current corona discharge," *IEEJ Trans. Electr. Electron. Eng.*, vol. 12, no. 1, pp. 16–23, Jan. 2017.
[10] X. M. Bian, H. Li, X. Zhang, X. Cui, T. Lu, and W. Song, "Influence of fine particulate matter on the variation of surface morphologies of conductors subjected to positive DC voltages," *Appl. Phys. Lett.*, vol. 113, no. 20, 2018, Art. no. 204112.
[11] W. Wang, L. Yang, K. Wu, C. Lin, P. Huo, S. Liu, D. Huang, and M. Lin, "Regulation-controlling of boundary layer by multi-wire-to-cylinder negative corona discharge," *Appl. Therm. Eng.*, vol. 119, pp. 438–448, Jun. 2017.
[12] E. Moreau and G. Touchard "Enhancing the mechanical efficiency of electric wind in corona discharges," *J. Electrostatics*, vol. 66, no. 1, pp. 39–44, Jan. 2008.
[13] R. T. Huang, W. J. Sheu, and C. C. Wang, "Heat transfer enhancement by needle-arrayed electrodes—An EHD integrated cooling system," *Energy Convers. Manage.*, vol. 50, no. 7, pp. 1789–1796, Jul. 2009.
[14] B. L. Owsenek, J. Seyed-Yagoobi, and R. H. Page, "Experimental investigation of corona wind heat transfer enhancement with a heated horizontal flat plate," *J. Heat Transf.*, vol. 117, no. 2, pp. 309–315, May 1995.
[15] A. Sahai, N. N. Mansour, B. Lopez, and M. Panesi, "Modeling of high pressure arc-discharge with a fully-implicit Navier–Stokes stabilized finite element flow solver," *Plasma Sources Sci. Technol.*, vol. 26, no. 5, 2017, Art. no. 055012.
[16] E. R. Kieft, J. J. van der Mullen, G. M. Kroesen, V. Banine, and K. N. Koshelev, "Characterization of a vacuum-arc discharge in tin vapor using time-resolved plasma imaging and extreme ultraviolet spectrometry," *Phys. Rev. E, Stat. Phys. Plasmas Fluids Relat. Interdiscip. Top.*, vol. 71, no. 2, Feb. 2005, Art. no. 026409.
[17] J. H. Geng, Y. Qin, F. Lv, X. Yao, and Y. Ding, "Electric field distribution and switching impulse discharge under shield ball surface scratch defect in an UHVDC hall," *Energies*, vol. 11, no. 6, p. 1408, 2018.
[18] K. O. Winter and M. J. Hargather, "Three-dimensional shock wave reconstruction using multiple high-speed digital cameras and background-oriented Schlieren imaging," *Exp. Fluids*, vol. 60, no. 6, p. 93, Jun. 2019.
[19] G. K. Sinha, S. Mahimkar, and A. Srivastava, "Schlieren-based simultaneous mapping of bubble dynamics and temperature gradients in nucleate flow boiling regime: Effect of flow rates and degree of subcooling," *Exp. Therm. Fluid Sci.*, vol. 104, pp. 238–257, Jun. 2019.
[20] E. Moreau, P. Audier, and N. Benard, "Ionic wind produced by positive and negative corona discharges in air," *J. Electrostatics*, vol. 93, pp. 85–96, Jun. 2018.
[21] V. T. Dau, T. X. Dinh, T. Terebessy, and T. T. Bui, "Ion wind generator utilizing bipolar discharge in parallel pin geometry," *IEEE Trans. Plasma Sci.*, vol. 44, no. 12, pp. 2979–2987, Dec. 2016.

FANGCHENG LV was born in Inner Mongolia, China, in 1963. He graduated from North China Electric Power University, majoring in power system and automation, in 2000, and received the doctor's degree in engineering. He is currently a Professor and a Doctoral Supervisor. He is mainly engaged in electrical equipment insulation mechanism, electrical equipment online monitoring and fault diagnosis, electrical equipment maintenance, and other aspects of research.

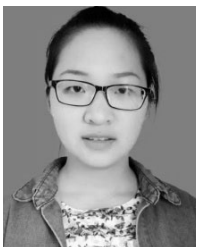

JINGXUAN SONG was born in 1995. She is currently pursuing the degree in high voltage and insulation technology with North China Electric Power University. Her main research interest includes high voltage and insulation technology space charge movement in ionic wind.

PING WANG was born in Sichuan, China, in 1982. She received the Ph.D. degree from North China Electric Power University, Baoding, China, in 2015. Her main research interests include the fields of electromagnetic compatibility and electromagnetic field theory and its application.

HAOOU RUAN was born in 1995. He is currently pursuing the degree in high voltage and insulation technology with North China Electric Power University. His main research interests include high voltage and insulation technology and electrical equipment insulation improvement.

JIANGHAI GENG was born in Hebei, China, in 1980. He received the B.Sc. degree from North China Electric Power University, Baoding, China, in 2007. His main research interests include the fields of high voltage and insulation technology and electromagnetic field theory and its application.